DOI: 10.1016/j.apsusc.2021.150403

Digging Ti interstitials at the *r*-TiO_2(110) surface: mechanism of porphyrin Ti sequestration by iminic N nucleophilic attack.

Markus K. Kremer,[a,b] Daniel Forrer,[a,d] Celia Rogero,[e] Luca Floreano,[f]* and Andrea Vittadini[a,d,g]*

[a] *Dipartimento di Scienze Chimiche, Università degli Studi di Padova, via Marzolo 1, I-35131, Padova, Italy*

[b] *Institute for Theoretical Physics, Justus Liebig University Giessen, Heinrich-Buff-Ring 16, D-35392 Gießen, Germany.*

[c] *Justus Liebig University Giessen, Heinrich-Buff-Ring 16, D-35392, Gießen, Germany.*

[d] *Istituto di Chimica della Materia Condensata e Tecnologie per l'Energia del Consiglio Nazionale delle Ricerche (CNR-ICMATE), via Marzolo 1, 35131, Padova, Italy.*

[e] *Materials Physics Center (CSIC-UPV/EHU), and Donostia International Physics Center (DIPC), Paseo Manuel de Lardizabal, 5 – E-20018 Donostia – San Sebastián , Spain.*

[f] *Istituto Officina dei Materiali del Consiglio Nazionale delle Ricerche (CNR-IOM), Laboratorio Nazionale TASC, I-34149 Trieste, Italy.*

[g] *INSTM UdR Padova, via Marzolo 1, I-35131, Padova, Italy.*

* e-mail: floreano@iom.cnr.it, andrea.vittadini@unipd.it

Abstract: Ti interstitials are key actors in the reduction/re-oxidation processes of TiO_2. The charge redistribution originated by these point defects is acknowledged to trigger the dissociation of small molecules at the surface, while the direct involvement of Ti interstitials in reactions with adsorbates is an open question. From a combined experimental and theoretical investigation, we show how the potential energy surface for the outdiffusion of Ti interstitials at rutile-TiO_2(110) is strongly lowered by adsorbed porphyrins, independently of their peripheral terminations. The process is activated by a nucleophilic attack of an iminic N to a surface 6-fold coordinated Ti atom, which is sequestrated by the porphyrin and replaced by a subsurface interstitial. From comparison with acidic porphyrins, we show that Ti extraction is specifically driven by the Lewis basicity of iminic N, which opens the pathway to the chemical reaction of Ti interstitials with a larger class of molecular systems.

Keywords: Titanium Dioxide; Ti interstitial defect; Porphyrin; On-surface molecular reaction; Self-Metalation; Minimum energy diffusion path.

Abbreviations: TBTPP, tetra-ditert-butyl-phenyl-porphyrin; TPP, tetra-phenyl-porphyrin; OEP, octa-ethyl-porphyrin; XPS, X-ray photoemission spectroscopy; STM, scanning tunneling microscopy; DFT, Density functional theory; MEP, minimum energy path; CI-NEB, climbing-image nudged elastic band.

1. Introduction

A large battery of molecules and ligands have been developed for the on-surface synthesis and modification of 2D molecular arrays, covalent organic frameworks, metal-organic coordination networks. The corresponding reaction processes are almost exclusively confined to a few metal surfaces,[1,2] which have the drawback of quenching to a more or less large extent the molecular electronic properties. Insulating substrates would allow electronic, or even mechanical, decoupling of the molecular assembly, but suitable synthesis strategies need to be developed. In this regard, titanium dioxide has been demonstrated to be a suitable playground for the synthesis of graphene nanoribbons,[3,4] graphene precursors,[5] as well as for polymerization.[6,7] TiO_2 owes its unique transport and catalytic properties to the possibility of injecting electrons into the, otherwise empty, Ti 3d band, which then falls below the Fermi level giving rise to a characteristic band gap state (BGS) and making the surface conductive and chemically reactive. Diverse mechanisms of populating the Ti 3d band are possible, from chemical reduction to doping. In particular, point defects play a crucial role in determining the TiO_2 surface electronic properties. Among them, oxygen vacancies (V_O) and titanium interstitials (Ti_i) are most common, and are inevitably formed during the mechanical, thermal and chemical processing of samples. In the past, the attention has been mainly focused on oxygen vacancies, also because their presence on the most studied surface, the (110) of the rutile polymorph, is apparent in scanning tunneling microscopy (STM) images.[8] Comparably less studied are the more elusive Ti_i defects, even though their presence is unquestionable, as they self-assemble in crystallographic shear planes in the bulk[9] and in ordered arrays in the 1×2 surface reconstruction of heavily reduced TiO_2.[10]

The association of the BGS with Ti_i[11-13] rather than with V_O[14] has been debated for many years. Experimentally, both types of defects are found to generate the same distribution of charge on *r*-TiO_2(110),[15] which is localized at a few subsurface lattice sites independently of the mechanism of charge injection.[16,17] Theoretically, the BGS in *r*-TiO_2(110) is described as a polaron, irrespective of the nature of source defect.[18-20] The polaron degree of charge delocalization depends on the level of theory,[21] and it can be spatially decoupled from its source defect via a hopping mechanism.[22] As a consequence, the

transport properties result to be independent of the nature of the defect, whereas chemical reactions with surface V_O and subsurface Ti_i would follow different pathways and may yield different products. The most studied dissociation of molecular oxygen and water at *r*-TiO_2(110) results either in the annealing of oxygen vacancies at room temperature[23,24] or in the synthesis of TiO_x clusters by outdiffusion of Ti_i beyond 400 K.[11] The latter process is responsible of the phenomenon of regrowth (or growth from beneath) when *r*-TiO_2(110) is exposed to O_2 at high temperature.[25] The reductive C=C coupling of benzaldehyde has been also proposed to be catalyzed by Ti_i,[26] where TiO_x clusters are finally left as a byproduct of stilbene desorption upon annealing.[27] In fact, these reactions only exploit the excess of charge manifested at the surface and do not require a physical involvement of Ti_i atoms. These are normally kept in the *r*-TiO_2(110) subsurface region because their energy is ~0.4 eV lower than at surface sites,[28] whereas oxygen vacancies are energetically more favourable at the surface than in deeper layers.[29] Only very recently, a direct involvement of Ti_i in the Ullmann's coupling reaction of polymer precursors has been proposed.[7] Here, we demonstrate the outdiffusion of Ti_i as the mechanism driving the metalation reaction of porphyrins on *r*-TiO_2(110). Metal atoms participating to this reaction can either be provided as reactants by e.g. vapor deposition,[30,31] or can be extracted from the surface upon thermal treatment (self-metalation reaction).[32] The latter process is quite effective on metals,[33-35] but has been recently observed also on a few insulators, such as the oxides of magnesium,[36,37] cobalt,[38-40] and titanium (both rutile[41,42] and anatase[43]). Here we find that metal-free porphyrins (2HP) lower the energy barrier for Ti_i outdiffusion, thus explaining the observed Ti incorporation in the porphyrin macrocycle at temperature values lower than 100˚C.[42]

2. Methods

2.1. Experimental

XPS measurements were performed at the Aloisa beamline of the Elettra Synchrotron in Trieste by means of a hemispherical analyzer in nearly normal emission with the sample at grazing incidence (4.0˚), corresponding to nearly p-polarization. STM images were measured in a different experimental setup at the CFM (CSIC/UPV-EHU) laboratory. Topographic images were collected at RT with a SPECS microscope (Aharus 150) equipped with a Colibri sensor tip, but operated in STM mode. Further experimental details can be found in Reference [42].

Commercially available free-base meso-substituted porphyrins were evaporated in UHV from homemade boron nitride crucibles, namely: 5,10,15,20-tetrakis(3,5-ditert-butylphenyl)-21H,23H-

porphine (CAS: 89372-90-7, purity >99%), 5,10,15,20-Tetraphenyl-21H,23H-porphine (CAS: 917-23-7, purity 99.5%) and 2,3,7,8,12,13,17,18-Octaethyl-21H,23H-porphine (CAS: 2683-82-1, purity 99.3%). We used a rate of deposition in the range of 0.2-05 Å/min as checked before and after deposition by quartz microbalances (both at Aloisa and in the STM setup). The Monolayer coverage was calibrated in advance from the XPS intensity, upon thermal desorption of a multilayer. The TiO_2(110) samples were purchased from Mateck, glued by silver paste to a Mo spacer, and prepared by Ar^+ sputtering at 0.8-1.0 kV, followed by flashes to ~1000 K. The temperature was determined by a thermocouple in direct contact with the Mo spacer at Aloisa; at the STM, the thermocouple was in contact with the clip locking the sample holder.

2.2. Calculations

Calculations were performed within a plane-wave pseudopotential framework, using the PWSCF code of the QUANTUM ESPRESSO suite (QE).[44] Valence orbitals were expanded on a plane-wave basis set with kinetic energy cutoff of 25 Ry, while the cutoff on the augmentation density was 200 Ry. The PBE[45] exchange-correlation functional was adopted, with Hubbard *U* correction[46] to treat Ti d states. A comparative study of the specific choice of the *U* correction (2.3 eV) is provided in the Appendix. The dispersion interactions were included by means of the D2 Grimme method.[47] The interaction between ion cores and valence electrons was modeled by ultrasoft pseudopotentials, whose core include 1s orbitals for C, N and O, and 1s-2p orbitals for Ti.

Surfaces were modeled by means of a repeated slab approach with PBE-D2 theoretical lattice constants of the substrate,[48] already used in Reference [42]. As the peripheral terminations and the corresponding intermolecular interactions do not experimentally affect the metalation reaction, we have adopted the unit cell of the 2HTPP ordered phase for a model study of the diffusion of Ti interstitials at TiO_2 (110). Starting from ~0.5 ML, 2HTPP and 4HTPP molecules organize into domains with a $\begin{pmatrix} 2 & -2 \\ 1 & 4 \end{pmatrix}$ oblique supercell,[42] whose area is equivalent to that of 10 unit cells, i.e. 25% larger than that of the (2 × 4) supercell adopted in Reference [28]. To our knowledge, this is the smallest unit cell adopted by TPP films on TiO_2(110),[49] and so it is the most convenient for our purpose. Here, we increase the number of TiO_2 layers from four, as used in our previous calculations,[42] to six, because we verified that four-layer slabs are inadequate to describe the properties of subsurface interstitials. In this regard, it should be pointed out that the excess electrons generated by the Ti interstitial give rise to several polaronic states whose energies differ by as much as 0.3 eV, and are properly described by slabs thicker than those used here.[20] The two bottom layers are kept frozen during the geometry optimization runs. The model is made of 439 atoms (78 2HTPP atoms + 1 Ti interstitial + 120 TiO_2 units). Due to the large size of the surface

cell, a Γ-point integration scheme was used to sample the surface Brillouin zone. Transition states have been located using the CI-NEB algorithm.[50]

3. Results and Discussion

Experimentally, the metalation reaction of porphyrins can be monitored by X-ray photoemission spectroscopy (XPS) of the N 1s core level. The pyrrolic (NH) and iminic (-N=) nitrogen atoms of a free-base porphyrin yield two distinct N 1s XPS peaks (the pyrrolic component is shifted to higher binding energy with respect to the iminic one by ~2 eV). Independently of their peripheral functionalization, first layer porphyrins 2HP adsorbed on *r*-TiO_2(110) may spontaneously transform into their acidic counterpart 4HP by capture of residual hydrogen atoms on the surface and in the nearby subsurface layers at RT.[51]

Representative N 1s spectra are shown in Figure 1 for three different porphyrin moieties, tetra-ditert-butyl-phenyl-, tetra-phenyl- and octaethyl-porphyrin (TBTPP, TPP, OEP) in the monolayer range, where they are mostly in their acidic form. Upon mild annealing (even below 100˚C for low coverage[42]), the pristine N components evolve towards a single N 1s peak, at a binding energy slightly higher (~0.5 eV) than the iminic one, corresponding to the coordination of the four N atoms to a central Ti atom. We have previously found for the case of TPP, that the incorporated Ti atom is further coordinated to two O_{br} atoms underneath, forming a TiO_2-TPP complex with a Ti^{4+} oxidation state. Independently of the initial amount of acidic molecules (4HTPP), full metalation of the TPP film in the monolayer range is achieved at 200˚C.[42] Here we show that the same self-metalation reaction path is observed for TBTPP and OEP in the same temperature range (see Figure 1), indicating a common reaction mechanism.

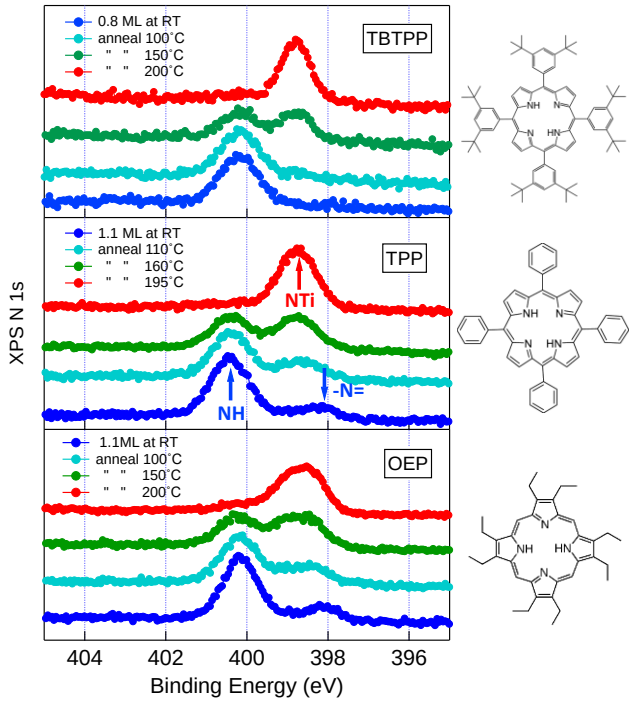

Figure 1. (*Color*) From top to bottom: the N 1s spectra (hv= 500 eV; ΔE~160 meV) of 2HTBTPP, 2HTPP and 2HOEP as deposited at RT (filled markers) and after annealing; the film coverage and annealing temperature are indicated in each graphic; arrows in the central panel (TPP) mark the binding energy of pyrrolic (NH), iminic (-N=) and metalated (NTi) nitrogen. The chemical structure of the free-base molecules is shown at the right side of the corresponding spectra.

The key configuration for the metalation process was found to be the 2HTPP adsorption on the O_{br} rows through anchoring of the pristine pyrrolic nitrogen atoms to the corresponding oxygen atoms underneath (NH•••O_{br} hydrogen bonds). Upon metalation, the TiO_2-TPP species preserve the same adsorption site, molecular orientation and intermolecular order of 2HTPP and 4HTPP. Remarkably, all of the three different molecular species (2HTPP, 4HTTP and TiO_2-TPP) also display the same intramolecular shape contrast, thus preventing their discrimination by STM, in full agreement with DFT simulations.[42] Topographic STM images confirm the O_{br} rows to be the preferred adsorption site also for 2HTBTPP molecules (see Figure 2). Even in absence of intermolecular lateral correlation, 2HTBTPP molecules display the same adsorption configuration of 2HTPP and the same critical temperature of metalation, suggesting a negligible role of the peripheral terminations and molecular ordering on the Ti incorporation mechanism. Considering the identical spectroscopic fingerprint and temperature behaviour, 2HOEP is also expected to follow the same kind of adsorption and metalation path. We may thus assume TPP molecules as a representative case of the general behavior of free-base porphyrins on *r*-TiO_2(110) and focus our theoretical analysis on this system, whose monolayer phase displays long range order with a commensurate $\begin{pmatrix} 2 & -2 \\ 1 & 4 \end{pmatrix}$ symmetry.

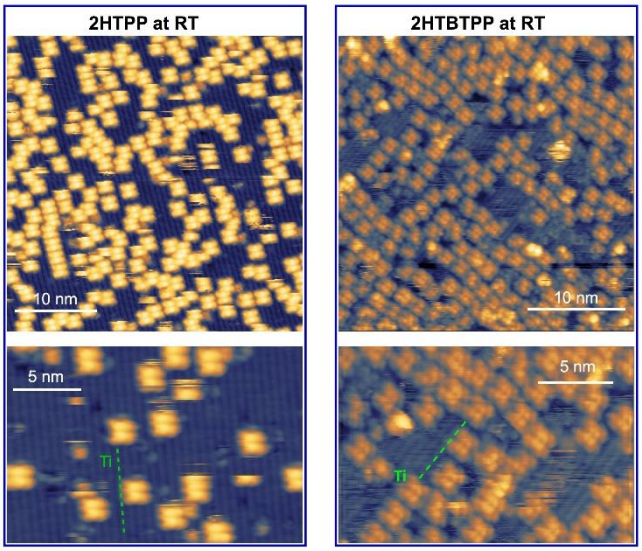

Figure 2. (*Color*) Left: STM images of 2HTPP deposited at RT (60 pA, -1.5 V): no long range ordering is observed at such a low coverage, whereas a $\begin{pmatrix} 2 & -2 \\ 1 & 4 \end{pmatrix}$ long range ordered phase sets in at 0.4-0.5 ML.[42] All molecules display a characteristic saddle-shape inflection (transverse to the rows) and 2HTPP molecules cannot be discriminated from their acidic counterpart 4HTPP.[51] Ti rows appear as bright stripes at both positive and negative bias, as highlighted in the bottom image. 2HTPP molecules lie on the dark stripes (O_{br} rows). Right: STM images of 2HTBTPP deposited at RT (90 pA, +1.3 eV); these molecules do not display the onset of long range order at any coverage; apart from a larger footprint of the peripheral terminations, 2HTBTPP displays the same in-plane orientation and conformational distortion (saddle-shape) like 2HTPP; as evidenced in the bottom image, 2HTBTPP molecules also adsorb atop the (dark) O_{br} rows.

We start our analysis by discussing the case of simply adsorbed 2HTPP molecules, then we will examine the case of doubly hydrogenated 4HTPP ones. In our DFT + *U* calculations of the energetics of porphyrin self-metalation, we assume that the reaction proceeds through three steps:

1. An *outdiffusion step*, where a near-surface interstitial Ti_i atom converts into a Ti adatom;

2. A *sequestration step*, where the adatom is captured by the porphyrin core, yielding a Ti@2HTPP(ads) complex;

3. An *H_2 recombination step*, where the pyrrolic hydrogen atoms finally desorb in the gas phase as a H_2 molecule.

Here, we neglect the step where a bulk interstitial diffuses to a near-surface interstitial site. In fact, it has been shown that the migration from the favored second layer site, which is ~0.1 eV more stable, requires a 0.84 eV barrier.[28] Furthermore, as we want to focus on the energetics of the extraction of Ti interstitials by the TPP film, we limit our study to processes (1) and (2). The energetics of the H_2 recombination step (3) will be addressed elsewhere.

With reference to drawings in Figure 3, we consider several positions for the extra Ti atom, including a sub-surface interstitial site (F) and two adatom sites, A and B. Type A sites are located at the side of the bridging oxygen (O_{br}) rows, in a position corresponding to a displaced short bridge site. In this way, the Ti adatom is bonded to two O_{br} and to one three-fold coordinated oxygen atom (O_{3c}). Type B sites are also located at the side of O_{br} row, but involve the coordination to one O_{br} and two O_{3c} atoms (see Figure 3a). The energy barriers for the outdiffusion of Ti interstitials at TiO_2(110) were formerly studied by DFT + *U* calculations by Mulheran et al.,[28] who found that F is the most stable subsurface site, approximately located below A. Analogous minima are located below the B surface sites. Sites A are more stable than B ones by 0.34 eV, but are less stable than subsurface F sites by 0.57 eV. Overall, the picture emerging from former calculations indicates that Ti interstitials are confined in the bulk by thermodynamics, where the lowest barrier for outdiffusion is 1.40 eV. This involves the conversion of an interstitial atom in site F into an adatom in site A.[28] *A priori*, this energy barrier would exclude a direct role of interstitial Ti atoms in the self-metalation reaction of porphyrins at temperatures as low as 100˚C.[36]

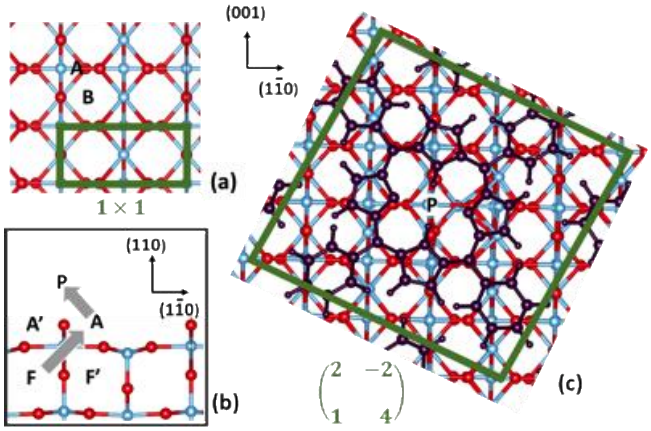

Figure 3. (*Color*) (a) Top and (b) side views of the TiO_2(110) surface; (c) top view of the oblique supercell used in the present work, where the adsorbed 2HTPP film is also shown. Relevant sites for Ti are indicated. Ti atoms are blue, O atoms are red, all the 2HTPP atoms are black. The borders of the 1 × 1 unit cell and of the oblique supercell are marked with green lines. The gray arrows in (b) show the approximate path of Ti during the self-metalation reaction.

We have thus computed the relative stability of the F, A, and B sites, both in absence and presence of 2HTPP. In step 1, the molecule is adsorbed at an O_{br} short bridge site interacting through its pyrrolic N atoms with two O_{br} atoms.[51] We also consider an additional configuration, where Ti is coordinated to the adsorbed molecule, still holding its pyrrolic H atoms. This corresponds to the intermediate metalated porphyrin (step 2). We indicate the Ti site for this configuration as P. The relative energies of all the sites are reported in Table 1, while the optimized structures of selected configurations are depicted in Figure

4. Here and in the following, we take the energy of a slab containing a 2HTPP adsorbate and a sub-surface interstitial at F as a zero reference.

Table 1. Energies (eV) relative to the sub-surface interstitial site F of relevant Ti adatom sites at the TiO_2(110) surface in absence (TiO_2) and in presence of dense (2HTPP/4HTPP-TiO_2), as calculated assuming U = 2.3 eV.

	site A	site B	site P
TiO_2	0.61	1.25	-
2HTPP-TiO_2	-0.49[a]	- [a,b]	-1.23
4HTPP-TiO_2	0.23	-	1.33

[a] Only A and B sites close to the 2HTPP adsorption site have been considered. [b] Not a local minimum.

The energies of the configurations for the clean surface fairly agree with those of Reference [28], keeping in mind the differences i) in the functional, Perdew-Wang vs. PBE-D2 here, ii) in the Hubbard U correction, 3.0 eV vs 2.3 eV here (see Appendix for comparative calculations with U = 3.0 eV) , and iii) in the supercells, 2 × 4 vs. $\begin{pmatrix} 2 & -2 \\ 1 & 4 \end{pmatrix}$ here. Overall, the sub-surface interstitial F site is largely favored, while the surface A site is preferred over the B site. Adding the 2HTPP film inverts the relative stability of the A and F sites, while the A site is in turn unfavoured with respect to the P site by 0.75 eV. Thus, a robust thermodynamic driving force now exists for both the outdiffusion and the sequestration steps. In addition, the B site close to the porphyrin center is no longer a local minimum.

It should be emphasized that a self-metalation reaction in absence of Ti interstitials, where a regular Ti surface ion is simply extracted from the lattice, is strongly unfavorable. In this case, the formation of an A-type intermediate step for 2HTPP costs 1.3 eV, to be compared with the energy gain of 0.49 eV when a Ti interstitial is involved (see Table I). Furthermore, no P-type local minimum is predicted. These findings are clearly in contrast with the low temperature observed for the onset of the self-metalation reaction.

We now turn to study the energetics of the self-metalation reaction, limiting ourselves to the outdiffusion and the sequestration steps. As pointed out above, we assume that the outdiffusion step starts from a subsurface interstitial at site F and ends with an adatom at the A site. In preliminary calculations, we verified that an additional local minimum T is present along the F → A outdiffusion path, where the interstitial assumes a pseudo-tetrahedral coordination. We thus subdivide the diffusion step into two segments, i.e. F → T and T → A, while we schematically indicate the sequestration step as A → P. We

study the minimum energy path (MEP) for these segments with separate climbing-image nudged elastic band (CI-NEB) calculations. The whole MEP curve for a 2HTPP adsorbate is shown in Figure 4, where the structures of the relevant local minima and transition states are also sketched.

We start our discussion of the MEP curve by examining the F → T segment. The activation energy for the forward (backward) step is 0.65 (0.87) eV. The atomic structures of the T state (local minimum) and of the transition state TS1 (saddle point) show that the mechanism involves the displacement of two Ti atoms: a subsurface Ti_{6c} lattice atom (Ti-I, in blue in Figure 4) outdiffuses and an interstitial Ti atom (Ti-II, in green in Figure 4) replaces it. The subsurface Ti-I is first displaced from its bulk-like 6-fold coordination to a planar 3-fold coordination, whereas Ti-II is less perturbed and keeps its 6-fold interstitial coordination unchanged. In the subsequent TS1 → T segment, Ti-II loses part of its bonds adopting a pseudo-tetrahedral geometry, while Ti-I (now, an adatom) increases its coordination number from 3 to 4, and assumes a pyramidal geometry, forming a bond (d = 2.13 Å) with a porphyrin N atom (iminic one).

In the second part of the outdiffusion step (T → A segment) Ti-II moves toward the vacant 6-fold coordinated surface site, while Ti-I further moves towards the porphyrin core. The position of Ti-I in the A intermediate is quite similar to that predicted for the clean surface, but in this case the Ti-I adatom is further stabilized by an extra Ti-N bond (see Figure 4). The formation of this bond provides the driving force for the outdiffusion process, thus inverting the relative stability of the F and A sites. Another shallow minimum is actually present between T and A. Overall, because the energy barriers are low (~0.05 eV) in the forward direction, this segment is kinetically irrelevant, and we do not discuss it further.

Taken as a whole, the Ti outdiffusion step in the presence of 2HTPP involves a 0.65 eV barrier. This is less than half of the 1.40 eV value computed by DFT + U for the clean surface,[28] and it is also definitely lower than the 1.2 eV barrier predicted by DFT in the presence of adsorbed O_2.[11] Obviously, the trend of the barriers for inward diffusion of a Ti adatom to a sub-surface interstitial site is also reversed: 1.14 eV in presence of adsorbed 2HTPP, to be compared with 0.83 eV computed for the clean surface. It is worth noting that the 0.65 eV barrier for the outdiffusion step is also lower than that required for the diffusion from a deeper to a sub-surface interstitial site, which has been computed to be 0.75 eV in the presence of O_2,[11] and 0.84 eV for the clean surface.[28]

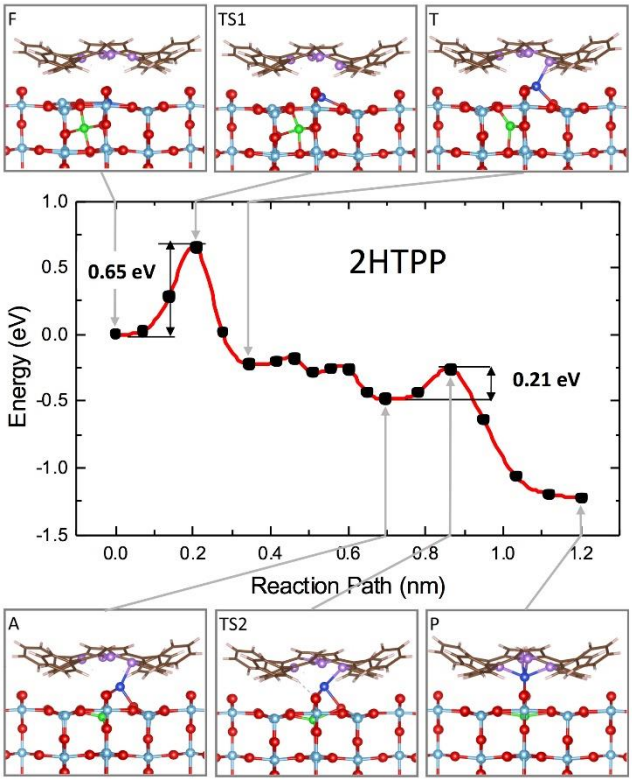

Figure 4. (*Color*) Minimum energy path (MEP) for the self-metalation reaction of 2HTPP adsorbed at TiO_2(110). Sketches of relevant configurations, viewed along [001], are shown in the gray boxes and are connected to the proper MEP point by arrows. O atoms are red, C atoms are brown, N atoms are purple, H atoms are white. Ti atoms are cyan, those involved in the diffusion process are blue (Ti-I) and green (Ti-II). Note the slight azimuthal rotation of the adsorbate due to the dense film packing. The red curve is a spline interpolation while black dots are the CI-NEB computed points.

The energy profile of the Ti sequestration step (A → P) is characterized by an activation energy for the forward (backward) step of 0.21 (0.96) eV. In this step, Ti-I, which is initially an adatom coordinated to a single N atom, is finally captured by the porphyrin, and assumes a pseudo-octahedral geometry, due to the coordination to two O_{br} ions and to the four porphyrin N atoms. Inspection of the geometries in the starting and transition states, A and TS2 (see Figure 4), reveals that the reaction mechanism proceeds first through a sort of 6-fold coordinated intermediate, where the Ti adatom interacts with three surface O atoms and three out of four N atoms.

Overall, the computed energetics is consistent with the observed onset of 2HTPP self-metalation reaction at temperatures of 100˚C. Remarkably, the whole chemical reaction does not significantly alter the photoemission spectra of the valence band and of the Ti 2p core level.[52] Since both the porphyrin incorporated Ti atoms and those in the bulk substrate have the same oxidation state (IV), we may conclude that the overall concentration of Ti interstitials (as monitored by the low binding energy tail of Ti 2p spectra) and the excess of charge (as monitored by the BGS intensity) in the layers closer to the surface

(as probed by the short excape depth of photoelectrons in the 100-200 eV range) do not change upon self-metalation. In fact, the outdiffusion process is driven by the gradient of chemical potential generated by the porphyrin self-metalation. Topmost Ti interstitials are first sequestrated by porphyrin metalation at mild temperature (barrier of 0.65 eV), then interstitials by deeper layers may outdiffuse at higher temperature (barrier of ~0.8 eV across bulk layers). This mechanism might also explain the observed lower temperature required for self-metalation at 0.2 ML:[42] at low coverage, molecules are not yet aggregated in domains and they can freely diffuse, hence reaching more easily the most reactive sites, i.e. those above the pristine Ti interstitials of the first subsurface layer.

We can now examine the case of doubly hydrogenated porphyrins, 4HTPP. These molecular species cannot be distinguished by STM topography from their neutral counterpart and they also display the same qualitative behaviour of 2HTPP in terms of absorption site,[51] molecular ordering,[42] phase transitions,[42] metalation reaction,[42] and final cyclo-dehydrogenation.[52] The MEP curve for the self-metalation reaction of 4HTPP (see Figure 5) is strongly changed with respect to that of the 2HTPP case. In fact, not only the overall process turns out to be endothermic by ~1.3 eV, but also the energy profile of the outdiffusion step is qualitatively modified and similar to that of the clean surface. This is because there is no longer an iminic N atom available for extra-coordination to a Ti adatom. In fact, the Ti adatom undergoes steric repulsions with the extra hydrogen atom just above it, and it is displaced below the heteroaromatic ring of the porphyrin macrocycle (see state A in Figure 5). These findings indicate that 4HTPP species, although able to lower somehow the energy landscape for Ti_i outdiffusion with respect to the clean surface, must release the excess hydrogen atoms prior to attract and sequestrate Ti interstitials. As an alternative, 4HTPP might release the two extra H atoms when the adatom has been already formed (intermediate stage A of Fig. 5). In either case, an activation energy for partial dehydrogenation must be taken into account. While investigating the details of porphyrin dehydrogenation goes beyond the scope of the present study, we remark that our theoretical results nicely agree with experimental evidence. A closer look at Figure 1 indicates that the -N= iminic components of the minority 2HP population present at RT readily disappears at 100˚C, while higher temperature annealing is required for full metalation of the 4HP majority population (NH peak). In fact, Köbl et al. reported a temperature of self-metalation about 100 K higher for 4HTPP than for 2HTPP,[41] which might account for the extra cost of the dehydrogenation step.

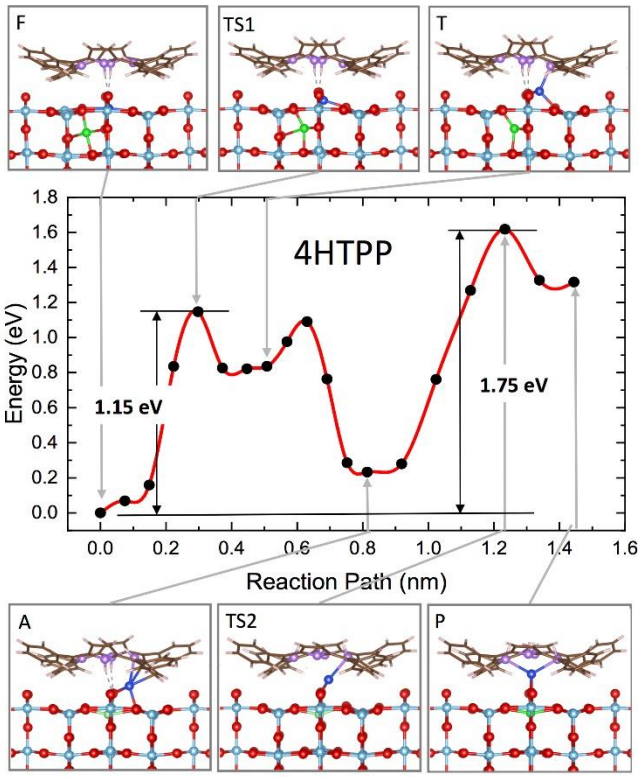

Figure 5. (*Color*) Minimum energy path (MEP) for the self-metalation reaction of 4HTPP adsorbed at TiO_2(110). Gray boxes show sketches of relevant configurations viewed along [001]. Colors as in Figure 4.

From the analysis of the 4HTPP MEP curve, we may draw some speculations about MTPP adsorption and the possibility of metal-exchange (trans-metalation), a phenomenon formerly reported to take place also on mildly reactive metal substrates,[53,54] which has relevant consequences on the hybrid interfaces for photovoltaic and magnetic applications. If MTPPs adsorb in the same configuration of 2H/4H/TiO_2-TPP, as effectively observed for Zn- and Cu-TPP,[55,56] we might expect that the interaction with the O_{br} rows may loosen to some extent the energy barriers and energy cost of creating an adatom A. In the case of 3d metals more reactive than Zn and Cu, the energetics might get closer to that of 4HTPP. However, the final step of metal exchange between the Ti adatom and the pristine metal of MTPP would remain the rate limiting process (whose energy cost has been evaluated in the range of 2 eV for Cu- and Co-phthalocyanines on copper[57]) because there are no free iminic N atoms to facilitate the adatom lifting, like for 4HTPP.

Going back to the 2HTPP case, an analysis of the MEP curve suggests an improved scheme for the first steps of the reaction. First of all, the reaction is triggered by a nucleophilic attack of an iminic nitrogen to the neighboring surface Ti_{6c} ion, which in turn is converted into a tetrahedrally coordinated Ti_{4c} ion leaving a Ti vacancy V_{Ti} (see configuration T of Fig. 2):

$Ti_{6c} \xrightarrow{2HTPP} Ti_{4c}(ads) + V_{Ti}$, (1′)

which is readily healed by a Ti interstitial (see configuration A of Fig. 2):

$V_{Ti} + Ti_i \rightarrow Ti_{6c}$. (1″)

Finally, the Ti_{4c} ion is sequestrated by the porphyrin, restoring its pseudo-octahedral coordination

$Ti_{4c}(ads) + 2HTPP(ads) \rightarrow Ti@2HTPP(ads)$, (2)

as shown in configuration P of Figure 4.

In the present case, none of above steps is rate determining, as all the associated barriers are lower in comparison to those involved in the interstitial diffusion from the bulk to the sub-surface region. However, the barrier of process (1″) is negligible, while that of (1′) is significantly higher than that of (2). This means that the Ti sequestration by the macrocycle, though highly exothermic, does not provide the driving force for the self-metalation reaction; rather, the key process of the self-metalation reaction is the nucleophilic attack, where Ti_{6c} is converted into Ti_{4c}. This is confirmed by the fact that when 2HTPP is replaced by 4HTPP, where all the iminic N atoms are converted into less nucleophilic pyrrolic ones, the outdiffusion of Ti_{6c} is no longer favored. Hence, we infer that the extraction of Ti interstitials at TiO_2(110) can be promoted by other Lewis bases adsorbed at the surface, i.e. that reactions involving Lewis bases at TiO_2(110) can form intermediate complexes with Ti adatoms.

4. Conclusions and Perspectives

In summary, we have shown that the mechanism of Ti self-metalation of porphyrins on the TiO_2(110) surface does not depend on the different peripheral terminations of the molecules and their mutual interactions, but only on the specific adsorption configuration of the tetrapyrrolic macrocycle atop the O_{br} rows. DFT + *U* calculations reveal that 2HTPP nitrogen atoms strongly modify the potential energy landscape, so that the outdiffusion of Ti interstitials turns from endo- to exothermic. By comparing the energetics of the Ti outdiffusion and of the Ti sequestration steps, we find that the former involves a higher barrier (0.65 eV vs. 0.21 eV), which is however lower than that previously computed for the diffusion from deeper to sub-surface interstitial sites (0.84 eV). These data are compatible with the experimental observation of the onset of self-metalation at temperatures below 100˚C.[42] Slightly higher heating is necessary to bring closer to the surface the Ti_i from deeper layers, thus continuing the metalation

reaction. The key mechanism for the outdiffusion is the interaction of a reticular Ti_{6c} beneath the O_{br} row with one of the iminic nitrogen atoms, which loosens the crystalline bonds and allows the outdiffusion of the Ti_{6c} atom and its replacement with a nearby interstitial Ti atom. In fact, when doubly hydrogenated 4HTPP species are rather considered, the adjacent nitrogen atoms are saturated and the residual interaction with the π-orbitals of the pyrrolic ring is not strong enough to make exothermic the Ti outdiffusion and sequestration. This explains the higher metalation temperature (~200˚C) required by the acidic species.[41] We might expect metal-TPPs adsorbed in the same configuration (like Zn- and Cu-TPP) to follow a thermodynamical trend similar to that of 4HTPP. A possible trans-metalation reaction with the substrate would thus require heating beyond 200˚C, well above the working temperature of solar panels, even in a sunny day. In a more general perspective, we provided the first evidence that Ti interstitials can be extracted from TiO_2 and incorporated into molecular structures other than oxide complexes, hence confirming that these defects can play a direct role in chemical reactions at the TiO_2 surface.

5. Appendix

Concerning the U parameter, it can be derived from first principles or from the fitting of some property (e.g. the host band gap) to an experimental or an "exact" theoretical value. Based on electronic structure features, Ti interstitials in rutile have been studied using values such as 2.5 eV,[58] 3 eV,[59] and 4.2 eV.[20] The larger U values better fit the energy location of the gap states,[18] however choosing U values in the 2—3 eV range is more appropriate, when studying redox processes involving TiO_2.[60] In particular, Lutfalla et al.[61] found $U = 2.3$ eV to reproduce quite well the experimental value for the reduction energy of TiO_2 to Ti_2O_3. Since in the present case we are also dealing with a change of oxidation state of Ti atoms (from a nominal Ti^{3+} interstitial to a nominal Ti^{4+} coordinated to porphyrin), we also adopted the $U = 2.3$ eV value. We additionally run calculations for a few specific configurations with $U = 3$ eV (see Table 2). The latter value slightly increases the stability ΔE of the A and B sites at the clean surface ($\Delta E = 0.51$ and 1.05 eV for A and B, respectively), in better agreement with Reference [28]. Calculations on the 2HTPP/TiO_2 system are less affected, as the relative stability of the A state is the same, whereas P is destabilized by 0.2 eV. Hence, the energetics of the system is not qualitatively modified by the choice of U.

Table 2. Energies (eV) relative to the sub-surface interstitial site F for Ti adatoms in sites A, B and P (see text) at the TiO_2(110) surface in absence (TiO_2) and in presence of a dense 2H-TPP film (TiO_2 + 2H-TPP), as calculated assuming U = 3.0 eV. Only A and B sites close to the 2H-TPP adsorption site have been considered.

System	Site		
	A	B	P
TiO_2	0.51	1.05	-
TiO_2[a]	0.57	0.91	-
TiO_2 + 2H-TPP	-0.49	- [b]	-1.02

[a] From Ref. [28] [b]Not a local minimum.

Author Contributions

L.F. and A.V. conceived the study and wrote the paper. M.K.K., D.F. and A.V. performed the calculations. C.R. and L.F. performed the experiments. L.F., A.V. and C.R. supervised the integration of experimental and theoretical data.

Acknowledgments

C.R. acknowledges funding from the Spanish Ministry of Economy and Competitiveness (grant MAT2016−78293−C6−5−R [AEI/ERDF, EU]) and from the Basque Government (grant IT − 1255 − 19). L.F. acknowledges funding's from the Italian Ministry of Research and University through EUROFEL project.

References

1. Clair, S.; De Oteyza, D. G. Controlling a Chemical Coupling Reaction on a Surface: Tools and Strategies for On-Surface Synthesis. Chem. Rev. 119 (2019) 4717-4776. https://doi.org/10.1021/acs.chemrev.8b00601.

2. Grill, L; Hecht, S. Covalent on-surface polymerization. Nat. Chem. 12 (2020) 115-130. https://doi.org/10.1038/s41557-019-0392-9.

3. Kolmer, M.; Zuzak, R.; Steiner, A. K.; Zajac, L.; Engelund, M.; Godlewski, S.; Szymonski, M.; Amsharov, K. Fluorine-Programmed Nanozipping to Tailored Nanographenes on Rutile TiO2 Surfaces. Science 363 (2019) 57-60. https://doi.org/10.1126/science.aav4954.

4. Kolmer, M.; Steiner, A.-K.; Izydorczyk, I.; Ko, W.; Engelund, M.; Szymonski, M.; Li, A.-P.; Amsharov, K. Rational Synthesis of Atomically Precise Graphene Nanoribbons Directly on Metal Oxide Surfaces. Science 369 (2020) 571-575. https://doi.org/10.1126/science.abb8880.

5. Sanchez-Sanchez, C.; Martinez, J. I.; Lanzilotto, V.; Biddau, G.; Gomez-Lor, B.; Perez, R.; Floreano, L.; Lopez, M.F.; Martin-Gago, J.A. Chemistry and Temperature-Assisted Dehydrogenation of C60H30 Molecules on TiO2(110) Surfaces. Nanoscale 5 (2013) 11058-11065. https://doi.org/10.1039/c3nr03706a.

6. Vasseur, G.; Abadia, M.; Miccio, L. A.; Brede, J.; Garcia-Lekue, A.; de Oteyza, D. G.; Rogero, C.; Lobo-Checa, J.; Ortega, J. E. Π Band Dispersion along Conjugated Organic Nanowires Synthesized on a Metal Oxide Semiconductor. J. Am. Chem. Soc. 138 (2016) 5685− 5692. https://pubs.acs.org/doi/10.1021/jacs.6b02151.

7. Abadia, M.; Vasseur, G.; Kolmer, M.; Zajac, L.; Verdini, A.; Ortega, J. E.; Floreano, L.; Rogero, C.; Brede, J. Increase of Polymerization Yield on Titania by Surface Reduction. J. Phys. Chem. C 124 (2020) 16918-16925. https://doi.org/10.1021/acs.jpcc.0c02125.

8. Minato, T.; Sainoo, Y.; Kim, Y.; Kato, H.; Aika, K.; Kawai, M.; Zhao, J.; Petek, H.; Huang, T.; He, W.; Wang, B.; Wang, Z.; Yan, Z.; Yang, J.; Hou, J. The Electronic Structure of Oxygen Atom Vacancy and Hydroxyl Impurity Defects on Titanium Dioxide (110) Surface. J. Chem. Phys. 130 (2009) 124502–124502. https://doi.org/10.1063/1.3082408.

9. Bursill, L. A.; Hyde, B. G. Crystallographic Shear in the Higher Titanium Oxides: Structure, Texture, Mechanisms and Thermodynamics. Progress in Solid State Chemistry 7 (1972) 177–253. https://doi.org/10.1016/0079-6786(72)90008-8.

10. Blanco-Rey, M.; Abad, J.; Rogero, C.; Mendez, J.; Lopez, M. F.; Martin-Gago, J. A.; de Andres, P. L. Structure of Rutile TiO2 (110)-(1×2): Formation of Ti2O3 Quasi-1D Metallic Chains. Phys. Rev. Lett. 96 (2006) 055502. https://doi.org/10.1103/PhysRevLett.96.055502.

11. Wendt, S.; Sprunger, P. T.; Lira, E.; Madsen, G. K. H.; Li, Z.; Hansen, J. Ø.; Matthiesen, J.; Blekinge-Rasmussen, A.; Lægsgaard, E.; Hammer, B.; Besenbacher, F. The Role of Interstitial

Sites in the Ti 3d Defect State in the Band Gap of Titania. Science 320 (2008) 1755. https://doi.org/10.1126/science.1159846.

12. Di Valentin, C.; Pacchioni, G.; Selloni, A. Reduced and n-Type Doped TiO2: Nature of Ti3+ Species. J. Phys. Chem. C 113 (2009) 20543–20552. https://doi.org/10.1021/jp9061797.

13. Finazzi, E.; Di Valentin, C.; Pacchioni, G. Nature of Ti Interstitials in Reduced Bulk Anatase and Rutile TiO2. J. Phys. Chem. C 113 (2009) 3382-3385. https://doi.org/10.1021/jp8111793.

14. Yim, C. M.; Pang, C. L.; Thornton, G. Oxygen Vacancy Origin of the Surface Band-Gap State of TiO_2(110). Phys. Rev. Lett. 104 (2010) 036806. https://doi.org/10.1103/PhysRevLett.104.036806.

15. Li, J.; Lazzari, R.; Chenot, S.; Jupille, J. Contributions of Oxygen Vacancies and Titanium Interstitials to Band-Gap States of Reduced Titania. Physical Review B 97 (2018) 041403. https://doi.org/10.1103/PhysRevB.97.041403.

16. Krüger, P.; Bourgeois, S.; Domenichini, B.; Magnan, H.; Chandesris, D.; Le Fèvre, P.; Flank, A. M.; Jupille, J.; Floreano, L.; Cossaro, A.; Verdini, A.; Morgante, A. Defect States at the TiO_2(110) Surface Probed by Resonant Photoelectron Diffraction. Phys. Rev. Lett. 100 (2008) 055501. https://doi.org/10.1103/PhysRevLett.100.055501.

17. Krüger, P.; Jupille, J.; Bourgeois, S.; Domenichini, B.; Verdini, A.; Floreano, L.; Morgante, A. Intrinsic Nature of the Excess Electron Distribution at the TiO2(110) Surface. Phys. Rev. Lett. 108 (2012) 126803. https://doi.org/10.1103/PhysRevLett.108.126803.

18. Deskins, N. A.; Rousseau, R.; Dupuis, M. Localized Electronic States from Surface Hydroxyls and Polarons in TiO_2(110). J. Phys. Chem. C 113 (2009) 14583–14586. https://doi.org/10.1021/jp9037655.

19. Kowalski, P. M.; Camellone, M. F.; Nair, N. N.; Meyer, B.; Marx, D. Charge Localization Dynamics Induced by Oxygen Vacancies on the TiO2 110 Surface. Phys. Rev. Lett. 105 (2010) 146405. https://doi.org/10.1103/PhysRevLett.105.146405.

20. Morita, K.; Shibuya, T.; Yasuoka, K. Stability of Excess Electrons Introduced by Ti Interstitial in Rutile TiO_2(110) Surface. J. Phys. Chem. C 121 (2017) 1602–1607. https://doi.org/10.1021/acs.jpcc.6b09669.

21. Chretien, S.; Metiu, H. Electronic Structure of Partially Reduced Rutile TiO2(110) Surface: Where Are the Unpaired Electrons Located? J. Phys. Chem. C 115 (2011) 4696-4705. https://doi.org/10.1021/jp111209a.

22. Deskins, N. A.; Dupuis, M. Electron transport via polaron hopping in bulk TiO2: A density functional theory characterization. Phys. Rev. B 75 (2007) 195212. https://doi.org/10.1103/PhysRevB.75.195212.

23. Du, Y.; Deskins, N. A.; Zhang, Z.; Dohnalek, Z.; Dupuis, M.; Lyubinetsky, I. Formation of O Adatom Pairs and Charge Transfer upon O2 Dissociation on Reduced TiO_2(110). Phys. Chem. Chem. Phys. 12 (2010) 6337–6344. https://doi.org/10.1039/c000250j.

24. Wendt, S.; Matthiesen, J.; Schaub, R.; Vestergaard, E.; Laegsgaard, E.; Besenbacher, F.; Hammer, B. Formation and Splitting of Paired Hydroxyl Groups on Reduced TiO_2(110). Phys. Rev. Lett. 96 (2006) 066107. https://doi.org/10.1103/PhysRevLett.96.066107.

25. Park, K. T.; Pan, M.; Meunier, V.; Plummer, E. W. Reoxidation of TiO_2(110) via Ti Interstitials and Line Defects. Phys. Rev. B 75 (2007) 245415. https://doi.org/10.1103/PhysRevB.75.245415.

26. Benz, L.; Haubrich, J.; Quiller, R. G.; Jensen, S. C.; Friend, C. M. McMurry Chemistry on TiO_2(110): Reductive C=C Coupling of Benzaldehyde Driven by Titanium Interstitials. J. Am. Chem. Soc. 131 (2009) 15026–15031. https://doi.org/10.1021/ja905522c.

27. Benz, L.; Haubrich, J.; Jensen, S. C.; Friend, C. M. Molecular Imaging of Reductive Coupling Reactions: Interstitial-Mediated Coupling of Benzaldehyde on Reduced TiO_2(110). ACS Nano 5 (2011) 834–843. https://doi.org/10.1021/nn103144u.

28. Mulheran, P. A.; Nolan, M.; Browne, C. S.; Basham, M.; Sanvillee, E.; Bennett, R. A. Surface and Interstitial Ti Diffusion at the Rutile TiO_2(110) Surface. Phys. Chem. Chem. Phys. 12 (2010) 9763–9771. https://doi.org/10.1039/c002698k.

29. Li, H.; Guo, Y.; Robertson, J. Calculation of TiO_2 Surface and Subsurface Oxygen Vacancy by the Screened Exchange Functional. J. Phys. Chem. C 119 (2015) 18160–18166. https://doi.org/10.1021/acs.jpcc.5b02430.

30. Wang, C.; Fan, Q.; Hu, S.; Ju, H.; Feng, X.; Han, Y.; Pan, H.; Zhua, J.; Gottfried, J. M. Coordination Reaction between Tetraphenylporphyrin and Nickel on a TiO_2(110) Surface. Chem. Commun. 50 (2014) 8291–8294. https://doi.org/10.1039/c4cc02919d.

31. Marbach, H. Surface-Mediated in Situ Metalation of Porphyrins at the Solid–Vacuum Interface. Acc. Chem. Res. 48 (2015) 2649–2658. https://doi.org/10.1021/acs.accounts.5b00243.

32. Auwärter,W.; Weber-Bargioni, A.; Brink, S.; Riemann, A.; Schiffrin, A.; Ruben, M.; Barth, J.V. Controlled metalation of self-assembled porphyrin nanoarrays in two dimensions Chem. Phys. Chem. 8 (2007) 250-254. 10.1002/cphc.200600675.

33. González-Moreno, R.; Sánchez-Sánchez, C.; Trelka, M.; Otero, R.; Cossaro, A.; Verdini, A.; Floreano, L.; Ruiz-Bermejo, M.; García-Lekue, A.; Martín-Gago, J. Á.; Rogero, C. Following the Metalation Process of Protoporphyrin IX with Metal Substrate Atoms at Room Temperature. J. Phys. Chem. C 115 (2011) 6849–6854. https://doi.org/10.1021/jp200533a..

34. Dyer, M. S.; Robin, A.; Haq, S.; Raval, R.; Persson, M.; Klimeš, J. Understanding the Interaction of the Porphyrin Macrocycle to Reactive Metal Substrates: Structure, Bonding, and Adatom Capture. ACS Nano 5 (2011) 1831–1838. https://doi.org/10.1021/nn102610k.

35. Diller, K.; Papageorgiou, A. C.; Klappenberger, F.; Allegretti, F.; Barth, J. V.; Auwärter, W. In Vacuo Interfacial Tetrapyrrole Metallation. Chem. Soc. Rev. 45 (2016) 1629–1656. https://doi.org/10.1039/C5CS00207A.

36. Schneider, J.; Franke, M.; Gurrath, M.; Röckert, M.; Berger, T.; Bernardi, J.; Meyer, B.; Steinrück, H.-P.; Lytken, O.; Diwald, O. Porphyrin Metalation at MgO Surfaces: A Spectroscopic and Quantum Mechanical Study on Complementary Model Systems. Chemistry – A European Journal 22 (2016), 1744–1749. https://doi.org/10.1002/chem.201503661.

37. Egger, L.; Hollerer, M.; Kern, C. S.; Herrmann, H.; Hurdax, P.; Haags, A.; Yang, X.; Gottwald, A.; Richter, M.; Soubatch, S.; Tautz, F. S.; Koller, G.; Puschnig, P.; Ramsey, M. G.; Sterrer, M. Charge-Promoted Self-Metalation of Porphyrins on an Oxide Surface. Angew. Chem. Int. Ed. 60 (2020) 5078-5082. https://doi.org/10.1002/anie.202015187.

38. Wechsler, D.; Fernández, C. C.; Tariq, Q.; Tsud, N.; Prince, K. C.; Williams, F. J.; Steinrück, H.-P.; Lytken, O. Interfacial Reactions of Tetraphenylporphyrin with Cobalt-Oxide Thin Films. Chemistry – A European Journal 25 (2019) 13197–13201. https://doi.org/10.1002/chem.201902680.

39. Wähler, T.; Schuster, R.; Libuda, J. Surface Structure Controls Self-Metalation: In-Situ IR Studies of Anchored Porphyrins on Atomically-Defined Cobalt Oxide Surfaces. J. Phys. Chem. C 124 (2020) 21538–21548. https://doi.org/10.1021/acs.jpcc.0c06248.

40. Wang, C.; Wang, R.; Hauns, J.; Fauster, T. Self-Metalation of Porphyrins by Cobalt Oxide: Photoemission Spectroscopic Investigation. J. Phys. Chem. C 124 (2020) 14167–14175. https://doi.org/10.1021/acs.jpcc.0c01722.

41. Köbl, J.; Wang, T.; Wang, C.; Drost, M.; Tu, F.; Xu, Q.; Ju, H.; Wechsler, D.; Franke, M.; Pan, H.; Marbach, H.; Steinrück, H.-P.; Zhu, J.; Lytken, O. Hungry Porphyrins: Protonation and Self-Metalation of Tetraphenylporphyrin on TiO_2(110)-1 × 1. Chem. Select 1 (2016) 6103–6105. https://doi.org/10.1002/slct.201601398.

42. Lovat, G.; Forrer, D.; Abadia, M.; Dominguez, M.; Casarin, M.; Rogero, C.; Vittadini, A.; Floreano, L. On-Surface Synthesis of a Pure and Long-Range-Ordered Titanium(IV)-Porphyrin Contact Layer on Titanium Dioxide. J. Phys. Chem. C 121 (2017) 13738–13746. https://doi.org/10.1021/acs.jpcc.7b03157.

43. Schneider, J.; Berger, T.; Diwald, O. Reactive Porphyrin Adsorption on TiO_2 Anatase Particles: Solvent Assistance and the Effect of Water Addition. ACS Appl. Mater. Interfaces 10 (2018) 16836–16842. https://doi.org/10.1021/acsami.8b00894.

44. Giannozzi, P.; Andreussi, O.; Brumme, T.; Bunau, O.; Nardelli, M. B.; Calandra, M.; Car, R.; Cavazzoni, C.; Ceresoli, D.; Cococcioni, M.; Colonna, N.; Carnimeo, I.; Dal Corso, A.; de Gironcoli, S.; Delugas, P.; DiStasio, R. A., Jr.; Ferretti, A.; Floris, A.; Fratesi, G.; Fugallo, G.; Gebauer, R.; Gerstmann, U.; Giustino, F.; Gorni, T.; Jia, J.; Kawamura, M.; Ko, H.-Y.; Kokalj, A.; Küçükbenli, E.; Lazzeri, M.; Marsili, M.; Marzari, N.; Mauri, F.; Nguyen, N. L.; Nguyen, H.-V.; Otero-de-la-Roza, A.; Paulatto, L.; Poncé, S.; Rocca, D.; Sabatini, R.; Santra, B.; Schlipf, M.;

Seitsonen, A. P.; Smogunov, A.; Timrov, I.; Thonhauser, T.; Umari, P.; Vast, N.; Wu, X.; Baroni, S. Advanced Capabilities for Materials Modelling with QUANTUM ESPRESSO. Journal of Physics: Condensed Matter 29 (2017) 465901. https://doi.org/10.1088/1361-648x/aa8f79.

45. Perdew, J.; Burke, K.; Ernzerhof, M. Generalized Gradient Approximation Made Simple. Phys. Rev. Lett. 77 (1996) 3865–3868. https://doi.org/10.1103/PhysRevLett.77.3865.

46. Himmetoglu, B.; Floris, A.; de Gironcoli, S.; Cococcioni, M. Hubbard-Corrected DFT Energy Functionals: The LDA+U Description of Correlated Systems. International Journal of Quantum Chemistry 114 (2014) 14–49. https://doi.org/10.1002/qua.24521.

47. Grimme, S. Semiempirical GGA-Type Density Functional Constructed with a Long-Range Dispersion Correction. J. Comput. Chem. 27 (2006) 1787–1799. https://doi.org/10.1002/jcc.20495.

48. Forrer, D.; Vittadini, A. 2D vs. 3D Titanium Dioxide: Role of Dispersion Interactions. Chem. Phys. Lett. 516 (2011) 72–75. https://doi.org/10.1016/j.cplett.2011.09.053.

49. Zajac, L.; Olszowski, P.; Godlewski, S.; Bodek, L.; Such, B.; Jöhr, R.; Pawlak, R.; Hinaut, A.; Glatzel, T.; Meyer, E.; Szymonski, M. Self-Assembling of Zn Porphyrins on a (110) Face of Rutile TiO2–The Anchoring Role of Carboxyl Groups. Appl. Surf. Sci. 379 (2016) 277–281. https://doi.org/10.1016/j.apsusc.2016.04.069.

50. Henkelman, G.; Uberuaga, B. P.; Jónsson, H. A Climbing Image Nudged Elastic Band Method for Finding Saddle Points and Minimum Energy Paths. J. Chem. Phys. 113 (2000) 9901–9904. https://doi.org/10.1063/1.1329672.

51. Lovat, G.; Forrer, D.; Abadia, M.; Dominguez, M.; Casarin, M.; Rogero, C.; Vittadini, A.; Floreano, L. Hydrogen Capture by Porphyrins at the TiO_2(110) Surface. Physical Chemistry Chemical Physics 17 (2015) 30119–30124. https://doi.org/10.1039/c5cp05437k.

52. Lovat, G.; Forrer, D.; Abadia, M.; Dominguez, M.; Casarin, M.; Rogero, C.; Vittadini, A.; Floreano, L. Very High Temperature Tiling of Tetraphenylporphyrin on Rutile TiO_2(110). Nanoscale 9 (2017) 11694–11704. https://doi.org/10.1039/c7nr04093h.

53. Doyle, C. M.; Cunniffe, J. P.; Krasnikov, S. A.; Preobrajenski, A. B.; Li, Z.; Sergeeva, N. N.; Senge, M. O.; Cafolla, A. A. Ni–Cu ion exchange observed for Ni(II)–porphyrins on Cu(111). Chemm. Comm. 50 (2014) 3447-3449. https://doi.org/10.1039/c3cc48913b.

54. Rieger, A.; Schnidrig, S.; Probst, B.; Ernst, K.-H.; Wačkerlin, C. Ranking the Stability of Transition-Metal Complexes by On-Surface Atom Exchange. J. Phys. Chem. Lett. 8 (2017) 6193-6198. https://doi.org/10.1021/acs.jpclett.7b02834.

55. Rangan, S.; Ruggieri, C.; Bartynski, R.; Martínez, J. I.; Flores, F.; Ortega, J. Densely Packed ZnTPPs Monolayer on the Rutile TiO2(110)-(1 1) Surface: Adsorption Behavior and Energy Level Alignment. J. Phys. Chem. C 120 (2016) 4430-4437. https://doi.org/10.1021/acs.jpcc.5b12736.

56. Pawlak, R.; Sadeghi, A.; Jöhr, R.; Hinaut, A.; Meier, T.; Kawai, S.; Zajac, Ł.; Olszowski, P.; Godlewski, S.; Such, B.; Glatzel, T.; Goedecker, S.; Szymoński, M.; Meyer, E. Hydroxyl-Induced Partial Charge States of Single Porphyrins on Titania Rutile. J. Phys. Chem. C 121 (2017) 3607-3614. https://doi.org/10.1021/acs.jpcc.6b11873.

57. Shen, K.; Narsu, B.; Ji, G.; Sun, H.; Hu, J.; Liang, Z.; Gao, X.; Li, H.; Li, Z.; Song, B.; Jiang, Z.; Huang, H.; Wells, J. W.; Song, F. On-surface manipulation of atom substitution between cobalt phthalocyanine and the Cu(111) substrate. RSC Adv. 7 (2017) 13827-13835. http://dx.doi.org/10.1039/C7RA00636E.

58. Stausholm-Møller, J.; Kristoffersen, H.; Hinnemann, B.; Madsen, G.; Hammer, B. DFT+U Study of Defects in Bulk Rutile TiO_2. J. Chem. Phys. 133 (2010) 144708–144708. https://doi.org/10.1063/1.3492449.

59. Nolan, M.; Elliott, S. D.; Mulley, J. S.; Bennett, R. A.; Basham, M.; Mulheran, P. Electronic Structure of Point Defects in Controlled Self-Doping of the TiO_2 Surface: Combined Photoemission Spectroscopy and Density Functional Theory Study. Phys. Rev. B 77 (2008) 235424. https://doi.org/10.1103/PhysRevB.77.235424.

60. Hu, Z.; Metiu, H. Choice of U for DFT+U Calculations for Titanium Oxides. J. Phys. Chem. C 115 (2011) 5841–5845. https://doi.org/10.1021/jp111350u.

61. Lutfalla, S.; Shapovalov, V.; Bell, A. T. Calibration of the DFT/GGA+U Method for Determination of Reduction Energies for Transition and Rare Earth Metal Oxides of Ti, V, Mo, and Ce. J. Chem. Theory Comput. 7 (2011) 2218–2223. https://doi.org/10.1021/ct200202g.